Dominant contributions to the nucleon-nucleon interaction at sixth order of chiral perturbation theory

D. R. Entem,[1,*] N. Kaiser,[2,†] R. Machleidt,[3,‡] and Y. Nosyk[3]
[1]*Grupo de Física Nuclear, IUFFyM, Universidad de Salamanca, E-37008 Salamanca, Spain*
[2]*Physik Department T39, Technische Universität München, D-85747 Garching, Germany*
[3]*Department of Physics, University of Idaho, Moscow, Idaho 83844, USA*
(Received 16 May 2015; revised manuscript received 26 September 2015; published 7 December 2015)

We present the dominant two- and three-pion-exchange contributions to the nucleon-nucleon interaction at sixth order (next-to-next-to-next-to-next-to-next-to-leading order, N^{5}LO) of chiral perturbation theory. Phase shifts with orbital angular momentum $L \geqslant 4$ are given parameter free at this order and allow for a systematic investigation of the convergence of the chiral expansion. The N^{5}LO contribution is prevailingly repulsive and considerably smaller than the N^{4}LO one, thus, showing the desired trend towards convergence. Using low-energy constants that were extracted from an analysis of πN scattering at fourth order, the predictions at N^{5}LO are in excellent agreement with the empirical phase shifts of peripheral partial waves.

DOI: 10.1103/PhysRevC.92.064001 PACS number(s): 13.75.Cs, 21.30.−x, 12.39.Fe, 11.10.Gh

I. INTRODUCTION

The derivation of nuclear forces from chiral effective field theory has been a topic of active research for the past quarter century [1–17] (see also Refs. [18,19] for recent reviews). By 1998, the evaluation of the nucleon-nucleon (NN) interaction up to next-to-next-to-leading order (N^{2}LO, third order in small momenta) was completed [2–4] and, by 2003, these calculations were extended to N^{3}LO [5–11]. As it turned out, at N^{2}LO and N^{3}LO, one is faced with a surplus of attraction, in particular, when the low-energy constants (LECs) for subleading pion-nucleon couplings are applied consistently, as extracted from analyses of elastic πN scattering [3,4,10].[1] Finally, in 2014, this issue was picked up and calculations up to N^{4}LO were conducted [15]. It was shown that the 2π- and 3π-exchange contributions at N^{4}LO are prevailingly repulsive and, thus, are able to fully compensate the excessive attraction of the lower orders. However, it was also noticed that the N^{2}LO, N^{3}LO, and N^{4}LO contributions are all roughly of the same magnitude, raising legitimate concerns about the convergence of the chiral expansion of the NN potential.

It is, therefore, the purpose of the present paper to move on to the next order and to investigate the NN interaction at N^{5}LO (of sixth power in small momenta) with the goal of obtaining more insight into the convergence issue.

Besides this, the order N^{5}LO has other interesting features. At this order, a new set of NN-contact terms depending with the sixth power on momenta appears, bringing the total number of short-distance parameters to 50. This set includes then terms that contribute up to F waves.

However, the focus of the present paper is on peripheral partial waves with orbital angular momentum $L \geqslant 4$, which are exclusively ruled by the nonpolynomial pion-exchange expressions constrained by chiral symmetry. Hence, this investigation is a test of the implications of chiral symmetry for the NN interaction up to sixth order.

This paper is organized as follows: In Secs. II A, II B, and II C, we consider the two-, three-, and four-pion exchange contributions at sixth order and argue that some parts are negligibly small. The predictions for elastic NN scattering in peripheral partial waves are shown in Sec. III, and Sec. IV concludes the paper.

II. PION-EXCHANGE CONTRIBUTIONS TO THE NN INTERACTION AT N^{5}LO

This section is subdivided into three subsections in which we will consider various classes of two- and three-pion exchange diagrams. We will present arguments for neglecting the chiral four-pion exchange at this order.

Crucial ingredients to our calculations are the πN amplitudes at various orders. For this, we follow Ref. [20] where also the effective Langrangian up to fourth order is given, which defines the LECs c_i, $\bar{d}_i$, and $\bar{e}_i$ (cf. Table I, below). We use the standard definition for chiral orders, according to which the nth order scales with the nth power of m_π or an external momentum Q. Consistent with Ref. [20], we count $Q/M_N \sim Q^2/\Lambda_\chi^2$, where M_N denotes the nucleon mass and Λ_χ the chiral symmetry breaking scale.

Our semi-analytical results will be stated in terms of contributions to the momentum-space NN amplitudes in the center-of-mass system (CMS), which arise from the following general decomposition of the NN potential:

$$\begin{aligned} V(\vec{p}\,',\vec{p}\,) = {} & V_C + \boldsymbol{\tau}_1\cdot\boldsymbol{\tau}_2\, W_C \\ & + [V_S + \boldsymbol{\tau}_1\cdot\boldsymbol{\tau}_2\, W_S]\,\vec{\sigma}_1\cdot\vec{\sigma}_2 \\ & + [V_{LS} + \boldsymbol{\tau}_1\cdot\boldsymbol{\tau}_2\, W_{LS}]\, i\vec{S}\cdot(\vec{k}\times\vec{q}\,) \\ & + [V_T + \boldsymbol{\tau}_1\cdot\boldsymbol{\tau}_2\, W_T]\,\vec{\sigma}_1\cdot\vec{q}\;\vec{\sigma}_2\cdot\vec{q} \\ & + [V_{\sigma L} + \boldsymbol{\tau}_1\cdot\boldsymbol{\tau}_2\, W_{\sigma L}]\,\vec{\sigma}_1\cdot(\vec{q}\times\vec{k}\,)\,\vec{\sigma}_2\cdot(\vec{q}\times\vec{k}), \end{aligned} \tag{2.1}$$

*entem@usal.es
†nkaiser@ph.tum.de
‡machleid@uidaho.edu

[1]Note that in the N^{3}LO potential of Ref. [11] the subleading LEC c_3 was chosen (in terms of magnitude) on the low side ($c_3 = -3.2$ GeV^{-1}) to reduce the attractive central force.

TABLE I. Low-energy constants as determined in Ref. [20]. The sets GW and KH are based upon the πN partial wave analyses of Refs. [26] and [27], respectively. The c_i, $\bar{d}_i$, and $\bar{e}_i$ are in units of GeV^{-1}, GeV^{-2}, and GeV^{-3}.

	GW	KH
c_1	−1.13	−0.75
c_2	3.69	3.49
c_3	−5.51	−4.77
c_4	3.71	3.34
$\bar{d}_1+\bar{d}_2$	5.57	6.21
$\bar{d}_3$	−5.35	−6.83
$\bar{d}_5$	0.02	0.78
$\bar{d}_{14}-\bar{d}_{15}$	−10.26	−12.02
$\bar{e}_{14}$	1.75	1.52
$\bar{e}_{15}$	−5.80	−10.41
$\bar{e}_{16}$	1.76	6.08
$\bar{e}_{17}$	−0.58	−0.37
$\bar{e}_{18}$	0.96	3.26

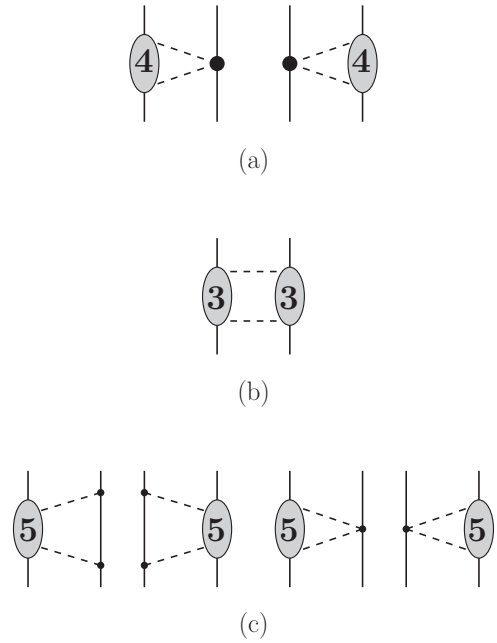

FIG. 1. Two-pion-exchange contributions to the NN interaction at N^{5}LO. (a) The subleading one-loop πN amplitude is folded with the chiral $\pi\pi NN$ vertices proportional to c_i. (b) The leading one-loop πN amplitude is folded with itself. (c) The leading two-loop πN amplitude is folded with the tree-level πN amplitude. Solid lines represent nucleons and dashed lines pions. Small dots and large solid dots denote vertices of chiral order 1 and 2, respectively. Shaded ovals represent complete πN-scattering amplitudes with their order specified by the number in the oval.

where $\vec{p}\,'$ and $\vec{p}$ denote the final and initial nucleon momenta in the CMS, respectively. Moreover, $\vec{q}=\vec{p}\,'-\vec{p}$ is the momentum transfer, $\vec{k}=(\vec{p}\,'+\vec{p})/2$ the average momentum, and $\vec{S}=(\vec{\sigma}_1+\vec{\sigma}_2)/2$ the total spin, with $\vec{\sigma}_{1,2}$ and $\boldsymbol{\tau}_{1,2}$ the spin and isospin operators of nucleon 1 and 2, respectively. For on-shell scattering, V_α and W_α ($\alpha=C,S,LS,T,\sigma L$) can be expressed as functions of $q=|\vec{q}\,|$ and $k=|\vec{k}|$ only. The one-pion exchange contribution is of the well-known form $W_T^{(1\pi)}=-(g_A/2f_\pi)^2(m_\pi^2+q^2)^{-1}$ with g_A the axial-vector coupling constant, $f_\pi=92.4\,\mathrm{MeV}$ the pion decay constant, and m_π the pion mass. Numerical values for g_A and m_π will be given in Sec. III. This expression fixes at the same time our sign convention for the NN potential $V(\vec{p}\,',\vec{p})$.

We will state contributions in terms of their spectral functions, from which the momentum-space amplitudes $V_\alpha(q)$ and $W_\alpha(q)$ are obtained via the subtracted dispersion integrals:

$$V_{C,S}(q)=\frac{2q^8}{\pi}\int_{nm_\pi}^{\tilde{\Lambda}}d\mu\,\frac{\mathrm{Im}\,V_{C,S}(i\mu)}{\mu^7(\mu^2+q^2)},$$
$$V_T(q)=-\frac{2q^6}{\pi}\int_{nm_\pi}^{\tilde{\Lambda}}d\mu\,\frac{\mathrm{Im}\,V_T(i\mu)}{\mu^5(\mu^2+q^2)}, \tag{2.2}$$

and similarly for $W_{C,S,T}$. The thresholds are given by $n=2$ for two-pion exchange and $n=3$ for three-pion exchange. For $\tilde{\Lambda}\to\infty$ the above dispersion integrals yield the finite parts of loop functions as in dimensional regularization, while for finite $\tilde{\Lambda}\gg nm_\pi$ we employ the method known as spectral-function regularization (SFR) [21]. The purpose of the finite scale $\tilde{\Lambda}$ is to constrain the imaginary parts to the low-momentum region where chiral effective field theory is applicable.

Before discussing the various groups of diagrams in detail, a general remark is in place concerning iterative diagrams. Iterative components occur for 2π as well as 3π exchanges and have to be subtracted. We perform these subtractions in the same way as was done for the planar 2π-exchange box diagram in Ref. [3]. The subtraction of iterative components in the 3π cases is explained in detail in Ref. [6].

A. Two-pion exchange contributions at N^{5}LO

The 2π-exchange contributions that occur at N^{5}LO are displayed graphically in Fig. 1. We will now discuss each class separately.

1. Spectral functions for 2π-exchange class (a)

The N^{5}LO 2π-exchange two-loop contributions, denoted by class (a), are shown in Fig. 1(a). For this class the spectral functions are obtained by integrating the product of the subleading one-loop πN amplitude (see Ref. [20] for details) and the chiral $\pi\pi NN$ vertex proportional to c_i over the Lorentz-invariant 2π-phase space. In the $\pi\pi$ center-of-mass frame this integral can be expressed as an angular integral $\int_{-1}^{1}dx$ [8]. Altogether, the results for the nonvanishing spectral

functions read

$$\begin{aligned}
\mathrm{Im}V_C &= \frac{m_\pi^6\sqrt{u^2-4}}{\left(8\pi f_\pi^2\right)^3}\left(\frac{1}{u^2}-2\right)[(c_2+6c_3)u^2+4(6c_1-c_2-3c_3)]\Big\{2c_1u+\frac{c_2u}{36}(5u^2-24)\\
&+\frac{c_3u}{2}(u^2-2)+\left[c_3(2-u^2)+\frac{c_2}{6}(4-u^2)-4c_1\right]\sqrt{u^2-4}\,B(u)\Big\}\\
&+\frac{m_\pi^6\sqrt{u^2-4}}{8\pi f_\pi^4 u}\Big\{[4c_1+c_3(u^2-2)]\left[\bar{e}_{15}(u^4-6u^2+8)+6\bar{e}_{14}(u^2-2)^2+\frac{3\bar{e}_{16}}{10}(u^2-4)^2\right]\\
&+c_2(u^2-4)\left[\frac{3\bar{e}_{15}}{10}(u^4-6u^2+8)+\bar{e}_{14}(u^2-2)^2+\frac{3\bar{e}_{16}}{28}(u^2-4)^2\right]\Big\}, \qquad (2.3)\\
\mathrm{Im}W_S &= \frac{c_4^2m_\pi^6(u^2-4)}{9\left(8\pi f_\pi^2\right)^3}\Big\{u\sqrt{u^2-4}\left[\frac{5u^2}{6}-4+\frac{2g_A^2}{15}(2u^2-23)\right]-(u^2-4)^2B(u)\\
&+6g_A^2u\int_0^1 dx\left(x-\frac{1}{x}\right)[4+(u^2-4)x^2]^{3/2}\ln\frac{x\sqrt{u^2-4}+\sqrt{4+(u^2-4)x^2}}{2}\Big\}\\
&+\frac{c_4m_\pi^6u(u^2-4)^{3/2}}{240\pi f_\pi^4}[10\bar{e}_{17}(2-u^2)+\bar{e}_{18}(4-u^2)]=\mu^2\,\mathrm{Im}W_T, \qquad (2.4)
\end{aligned}$$

with the dimensionless variable $u=\mu/m_\pi>2$ and the logarithmic function

$$B(u)=\ln\frac{u+\sqrt{u^2-4}}{2}\,. \qquad (2.5)$$

Consistent with the calculation of the πN-amplitude in Ref. [20], we utilized the relations between the fourth-order LECs, such that only $\bar{e}_{14}$ to $\bar{e}_{18}$ remain in the final result.

2. Spectral functions for 2π-exchange class (b)

A first set of 2π-exchange contributions at three-loop order, denoted by class (b), is displayed in Fig. 1(b). For this class of diagrams, the leading one-loop πN-scattering amplitude is multiplied with itself and integrated over the 2π-phase space. Including also the symmetry factor $1/2$, one gets for the spectral functions

$$\begin{aligned}
\mathrm{Im}V_C &= \frac{m_\pi^6\sqrt{u^2-4}}{(4f_\pi)^8\pi^3u}\Big\{-\frac{3}{70}(5u^2+8)(u^2-4)^2+3g_A^2(1-2u^2)\left[1+\frac{2-u^2}{4u}\ln\frac{u+2}{u-2}\right]\\
&\times\left[u-\frac{u^3}{2}+\frac{4B(u)}{\sqrt{u^2-4}}\right]+g_A^4\Big[\frac{32(3-2u^2)}{\sqrt{u^2-4}}B(u)+3(2u^2-1)^2\Big(\frac{u^2-2}{u}\ln\frac{u+2}{u-2}\\
&+\frac{(u^2-2)^2}{8u^2}\Big(\pi^2-\ln^2\frac{u+2}{u-2}\Big)\Big)-\frac{2258}{35}+24u+\frac{5336u^2}{105}-12u^3-\frac{2216u^4}{105}+\frac{18u^6}{35}\Big]\\
&+g_A^6(2u^2-1)\Big(1+\frac{2-u^2}{4u}\ln\frac{u+2}{u-2}\Big)\Big[46u-3u^3-96+\frac{64}{u+2}+\frac{24(5-2u^2)}{\sqrt{u^2-4}}B(u)\Big]\\
&+\frac{64g_A^8}{9}\Big[\frac{3119u^2}{70}-\frac{71u^6}{1120}-\frac{197u^4}{70}-\frac{85u^3}{8}+\frac{97u}{4}-\frac{582}{7}-\frac{16}{u+2}+\frac{8}{(u+2)^2}+\frac{6u^4-60u^2+105}{\sqrt{u^2-4}}B(u)\Big]\Big\}, \qquad (2.6)\\
\mathrm{Im}W_S &= \frac{g_A^4m_\pi^6\sqrt{u^2-4}}{(4f_\pi)^8\pi^3u}\Big\{\frac{u^2-4}{48}\Big[4u+(4-u^2)\ln\frac{u+2}{u-2}\Big]^2-\frac{\pi^2}{48}(u^2-4)^3\\
&+g_A^2u\Big[(u^2-4)\ln\frac{u+2}{u-2}-4u\Big]\Big[\frac{5u}{4}-\frac{u^3}{24}-\frac{8}{3}+\frac{5-u^2}{\sqrt{u^2-4}}B(u)\Big]\\
&+\frac{32g_A^4u^2}{27}\Big[\frac{u^4}{40}+\frac{13u^2}{10}+\frac{11u}{2}-\frac{118}{5}-\frac{8}{u+2}+\frac{3(10-u^2)}{\sqrt{u^2-4}}B(u)\Big]\Big\}=\mu^2\mathrm{Im}W_T, \qquad (2.7)
\end{aligned}$$

$$\mathrm{Im}V_S = \frac{g_A^8 m_\pi^6 u\sqrt{u^2-4}}{3(4f_\pi)^8\pi^5}\int_0^1 dx\,(x^2-1)\Big\{(u^2-4)x\Big[\frac{48\pi^2 f_\pi^2}{g_A^4}(\bar d_{14}-\bar d_{15})-\frac{1}{6}\Big]+\frac{4}{x}$$
$$-\frac{[4+(u^2-4)x^2]^{3/2}}{x^2\sqrt{u^2-4}}\ln\frac{x\sqrt{u^2-4}+\sqrt{4+(u^2-4)x^2}}{2}\Big\}^2=\mu^2\mathrm{Im}V_T, \tag{2.8}$$

$$\mathrm{Im}W_C = -\frac{m_\pi^6(u^2-4)^{5/2}}{(4f_\pi)^8(3\pi u)^3}\Big[2+4g_A^2-\frac{u^2}{2}\big(1+5g_A^2\big)\Big]^2+\frac{m_\pi^6(u^2-4)^{3/2}}{9(4f_\pi)^8\pi^5 u}\int_0^1 dx\,x^2\Big\{\frac{3x^2}{2}(4-u^2)$$
$$+3x\sqrt{u^2-4}\sqrt{4+(u^2-4)x^2}\ln\frac{x\sqrt{u^2-4}+\sqrt{4+(u^2-4)x^2}}{2}+g_A^4[(4-u^2)x^2$$
$$+2u^2-4]\Big[\frac{5}{6}+\frac{4}{(u^2-4)x^2}-\Big(1+\frac{4}{(u^2-4)x^2}\Big)^{3/2}\ln\frac{x\sqrt{u^2-4}+\sqrt{4+(u^2-4)x^2}}{2}\Big]$$
$$+\big[4\big(1+2g_A^2\big)-u^2\big(1+5g_A^2\big)\big]\sqrt{u^2-4}\,\frac{B(u)}{u}+\frac{u^2}{6}\big(5+13g_A^2\big)-4\big(1+2g_A^2\big)$$
$$+96\pi^2 f_\pi^2[(4-2u^2)(\bar d_1+\bar d_2)+(4-u^2)x^2\bar d_3+8\bar d_5]\Big\}^2. \tag{2.9}$$

Note the squared integrands in the last two equations. The parameters $\bar d_j$ belong to the $\pi\pi NN$-contact vertices of third chiral order.

3. 2π class (c)

Further 2π-exchange three-loop contributions at N^{5}LO, denoted by class (c), are shown in Fig. 1(c). For these the two-loop πN-scattering amplitude (which is of order 5) would have to be folded with the tree-level πN amplitude. To our knowledge, the two-loop elastic πN-scattering amplitude has never been evaluated in a decent analytical form. Note that the loops involved in the class (c) contributions include only leading order chiral πN vertices. According to our experience such contributions are typically small. For these reasons we omit class (c) in the present calculation.

4. Relativistic $1/M_N^2$ corrections

This group consists of the $1/M_N^2$ corrections to the chiral leading 2π-exchange diagrams. Representative graphs are shown in Fig. 2. Since we count $Q/M_N \sim (Q/\Lambda_\chi)^2$, these relativistic corrections are formally of sixth order (N^{5}LO). The expressions for the corresponding NN amplitudes are adopted from Ref. [9]:

$$V_C = \frac{g_A^4}{32\pi^2 M_N^2 f_\pi^4}\Big[L(\tilde\Lambda;q)\big(2m_\pi^4+q^4-8m_\pi^6 w^{-2}-2m_\pi^8 w^{-4}\big)-\frac{m_\pi^6}{2w^2}\Big], \tag{2.10}$$

$$W_C = \frac{1}{192\pi^2 M_N^2 f_\pi^4}\Big\{L(\tilde\Lambda;q)\big[g_A^2\big(2k^2\big(8m_\pi^2+5q^2\big)+12m_\pi^6 w^{-2}-3q^4-6m_\pi^2 q^2-6m_\pi^4\big)+g_A^4\big(k^2\big(16m_\pi^4 w^{-2}-20m_\pi^2-7q^2\big)$$
$$-16m_\pi^8 w^{-4}-12m_\pi^6 w^{-2}+4m_\pi^4 q^2 w^{-2}+5q^4+6m_\pi^2 q^2+6m_\pi^4\big)+k^2 w^2\big]-\frac{4g_A^4 m_\pi^6}{w^2}\Big\}, \tag{2.11}$$

$$V_T = -\frac{1}{q^2}V_S = \frac{g_A^4\,L(\tilde\Lambda;q)}{32\pi^2 M_N^2 f_\pi^4}\Big(k^2+\frac{5}{8}q^2+m_\pi^4 w^{-2}\Big), \tag{2.12}$$

$$W_T = -\frac{1}{q^2}W_S = \frac{L(\tilde\Lambda;q)}{1536\pi^2 M_N^2 f_\pi^4}\big[g_A^4\big(28m_\pi^2+17q^2+16m_\pi^4 w^{-2}\big)-2g_A^2\big(16m_\pi^2+7q^2\big)+w^2\big], \tag{2.13}$$

$$V_{LS} = \frac{g_A^4\,L(\tilde\Lambda;q)}{128\pi^2 M_N^2 f_\pi^4}\big(11q^2+32m_\pi^4 w^{-2}\big), \tag{2.14}$$

$$W_{LS} = \frac{L(\tilde\Lambda;q)}{256\pi^2 M_N^2 f_\pi^4}\Big[2g_A^2\big(8m_\pi^2+3q^2\big)+\frac{g_A^4}{3}\big(16m_\pi^4 w^{-2}-11q^2-36m_\pi^2\big)-w^2\Big], \tag{2.15}$$

$$V_{\sigma L} = \frac{g_A^4\,L(\tilde\Lambda;q)}{32\pi^2 M_N^2 f_\pi^4}\,, \tag{2.16}$$

where the (regularized) logarithmic loop function is given by

$$L(\tilde{\Lambda};q)=\frac{w}{2q}\ln\frac{\tilde{\Lambda}^2\left(2m_\pi^2+q^2\right)-2m_\pi^2q^2+\tilde{\Lambda}\sqrt{\tilde{\Lambda}^2-4m_\pi^2}\,q\,w}{2m_\pi^2(\tilde{\Lambda}^2+q^2)}, \tag{2.17}$$

with the abbreviation $w=\sqrt{4m_\pi^2+q^2}$.

B. Three-pion exchange contributions at N^{5}LO

The 3π-exchange contributions of order N^{5}LO are shown in Fig. 3. We can distinguish between diagrams which are proportional to c_i^2 [Fig. 3(a)] and contributions that involve (parts of) the leading one-loop πN amplitude [Fig. 3(b)]. Below, we present the spectral functions for each class.

1. Spectral functions for 3π-exchange class (a)

This class consists of the diagrams displayed in Fig. 3(a). They are characterized by the presence of one subleading $\pi\pi NN$ vertex in each nucleon line. Using a notation introduced in Refs. [7,15], we distinguish between the various subclasses of diagrams by roman numerals.

Class XIa:

$$\mathrm{Im}W_C=\frac{g_A^2c_4^2m_\pi^6}{6\left(4\pi f_\pi^2\right)^3}\int_2^{u-1}dw\,(w^2-4)^{3/2}\sqrt{\lambda(w)}, \tag{2.18}$$

$$\begin{aligned}\mathrm{Im}V_S=&\frac{g_A^2c_4^2m_\pi^6}{6\left(8\pi f_\pi^2\right)^3}\int_2^{u-1}dw\,\frac{(w^2-4)^{3/2}}{u^4\sqrt{\lambda(w)}}[w^8-4(1+u^2)w^6+2w^4(3+5u^2)\\&+4w^2(2u^6-5u^4-2u^2-1)-(u^2-1)^3(5u^2+1)],\end{aligned} \tag{2.19}$$

$$\mathrm{Im}(\mu^2V_T-V_S)=\frac{g_A^2c_4^2m_\pi^6}{6\left(8\pi f_\pi^2\right)^3}\int_2^{u-1}dw\,(w^2-4)^{3/2}\sqrt{\lambda(w)}\left[\frac{(w^2-1)^2}{u^4}+1-\frac{2}{u^2}(7w^2+1)\right], \tag{2.20}$$

with the kinematical function $\lambda(w)=w^4+u^4+1-2(w^2u^2+w^2+u^2)$. The dimensionless integration variable w is the invariant mass of a pion-pair divided by m_π.

Class XIIa:

$$\mathrm{Im}V_C=\frac{g_A^2c_4^2m_\pi^6}{8960\pi f_\pi^6}(u-3)^3\left[u^3+9u^2+12u-3-\frac{3}{u}\right], \tag{2.21}$$

$$\mathrm{Im}W_C=\frac{2g_A^2c_4^2m_\pi^6u^2}{\left(4\pi f_\pi^2\right)^3}\iint_{z^2<1}d\omega_1d\omega_2\,k_1k_2\sqrt{1-z^2}\arcsin(z), \tag{2.22}$$

$$\begin{aligned}\mathrm{Im}V_s=&\frac{g_A^2c_4^2m_\pi^6}{\left(4\pi f_\pi^2\right)^3}\iint_{z^2<1}d\omega_1d\omega_2\left\{2\omega_1^2\left(\omega_2^2-9\omega_2u+9u^2+1\right)+3\omega_1[\omega_2(1+8u^2)-6u-6u^3]\right.\\&+\frac{1}{4}(9u^4+18u^2+5)+\frac{2zk_2}{k_1}\left[\omega_1^3(4u-\omega_2)+\omega_1^2(7\omega_2u-2-2u^2)-2\omega_1(2u+\omega_2)+2+2u^2-4\omega_2u\right]\\&+\frac{3\arcsin(z)}{k_1k_2\sqrt{1-z^2}}\left[2\omega_1^3u(u^2+1-2\omega_2u)+\omega_1^2\left(\omega_2u(7+11u^2)-5\omega_2^2u^2-1-4u^2-3u^4\right)\right.\\&\left.\left.+\frac{\omega_1}{4}(6u^5+12u^3-2u-\omega_2(5+16u^2+15u^4))+\frac{(1-u^4)(u^2+3)}{8}\right]\right\},\end{aligned} \tag{2.23}$$

$$\begin{aligned}\mathrm{Im}(\mu^2V_T-V_S)=&\frac{g_A^2c_4^2m_\pi^6}{(4\pi f_\pi^2)^3}\iint_{z^2<1}d\omega_1d\omega_2\left\{4\omega_1^2\left(\omega_2^2+6u^2+2-10\omega_2u\right)+6u^2(1+u^2)\right.\\&+2\omega_1[3\omega_2(1+7u^2)-18u^3-10u]+\frac{2zk_2}{k_1}\left[\omega_1^3(7u-2\omega_2)+u^2-\omega_2u\right.\\&\left.+\omega_1^2(13\omega_2u-3-10u^2)+\omega_1(2+3u^2)(u-2\omega_2)\right]+\frac{3\arcsin(z)}{k_1k_2\sqrt{1-z^2}}\\&\left.\times(u^2-2\omega_1u+1)(u^2-2\omega_2u+1)\left[\frac{\omega_1}{2}(6u-5\omega_2)-\frac{u^2}{2}-2\omega_1^2\right]\right\},\end{aligned} \tag{2.24}$$

with the magnitudes of pion momenta divided by m_π, and their scalar product given by

$$k_1 = \sqrt{\omega_1^2 - 1}, \qquad k_2 = \sqrt{\omega_2^2 - 1}, \qquad z\,k_1 k_2 = \omega_1\omega_2 - u(\omega_1 + \omega_2) + \frac{u^2+1}{2}\,. \tag{2.25}$$

The upper/lower limits of the ω_2-integration are $\omega_2^\pm = \frac{1}{2}(u - \omega_1 \pm k_1\sqrt{u^2 - 2\omega_1 u - 3}/\sqrt{u^2 - 2\omega_1 u + 1}\,)$ with ω_1 in the range $1 < \omega_1 < (u^2-3)/2u$.

The contributions to $\mathrm{Im}W_S$ and $\mathrm{Im}(\mu^2 W_T - W_S)$ are split into three pieces according to their dependence on the isoscalar and isovector low-energy constants $c_{1,3}$ and c_4:

$$\mathrm{Im}W_S = \frac{g_A^2 m_\pi^6 (u-3)^2}{2240\pi f_\pi^6}\left\{7c_1^2\left(\frac{4}{3} + \frac{3}{u} - \frac{2}{3u^2} - \frac{1}{u^3}\right) + c_1 c_3\left(\frac{2u^2}{3} + 4u - \frac{2}{3} - \frac{5}{u} - \frac{2}{3u^2} - \frac{1}{u^3}\right)\right.$$
$$\left. + c_3^2\left(\frac{3u^2}{4} + \frac{u}{8} - \frac{5}{2} - \frac{3}{u} + \frac{19}{12u^2} + \frac{19}{8u^3}\right)\right\}, \tag{2.26}$$

$$\mathrm{Im}(\mu^2 W_T - W_S) = \frac{g_A^2 m_\pi^6 (u-3)}{1120\pi f_\pi^6}\left\{7c_1^2\left(\frac{1}{3u} + \frac{1}{u^2} + \frac{3}{u^3} - 2u - 1\right) + c_1 c_3\left(13u + 4 - 5u^2 - \frac{5u^3}{3} + \frac{1}{3u} + \frac{1}{u^2} + \frac{3}{u^3}\right)\right.$$
$$\left. + \frac{c_3^2}{8}\left(23u^2 - \frac{u^5}{3} - u^4 - 4u^3 - 8u - 3 + \frac{8}{3u} - \frac{19}{u^2} - \frac{57}{u^3}\right)\right\}, \tag{2.27}$$

$$\mathrm{Im}W_S = \frac{g_A^2 c_4 m_\pi^6}{1120\pi f_\pi^6}(u-3)^2\left\{c_1\left(u^2 + 6u - 1 - \frac{15}{2u} - \frac{1}{u^2} - \frac{3}{2u^3}\right)\right.$$
$$\left. + \frac{c_3}{4}\left(\frac{2u^4}{9} + \frac{4u^3}{3} + \frac{u^2}{3} - \frac{25u}{6} + \frac{6}{u} + \frac{1}{u^2} + \frac{3}{2u^3}\right)\right\}, \tag{2.28}$$

$$\mathrm{Im}(\mu^2 W_T - W_S) = \frac{g_A^2 c_4 m_\pi^6}{1120\pi f_\pi^6}(u-3)^3\left\{c_1\left(\frac{1}{u^2} + \frac{1}{u^3} - \frac{u}{3} - 3 - \frac{4}{u}\right) + \frac{c_3}{4}\left(\frac{u^3}{9} + u^2 + \frac{5u}{3} + \frac{8}{3} + \frac{11}{3u} - \frac{1}{u^2} - \frac{1}{u^3}\right)\right\}, \tag{2.29}$$

$$\mathrm{Im}W_S = \frac{g_A^2 c_4^2 m_\pi^6}{8960\pi f_\pi^6}(u-3)^2\left(\frac{25u}{12} - \frac{u^4}{9} - \frac{2u^3}{3} - \frac{u^2}{6} - \frac{3}{u} - \frac{1}{2u^2} - \frac{3}{4u^3}\right), \tag{2.30}$$

$$\mathrm{Im}(\mu^2 W_T - W_S) = \frac{g_A^2 c_4^2 m_\pi^6}{8960\pi f_\pi^6}(u-3)^3\left(\frac{1}{2u^2} + \frac{1}{2u^3} - \frac{u^3}{18} - \frac{u^2}{2} - \frac{5u}{6} - \frac{4}{3} - \frac{11}{6u}\right). \tag{2.31}$$

2. *Spectral functions for 3π-exchange class (b)*

This class is displayed in Fig. 3(b). Each 3π-exchange diagram of this class includes the one-loop πN amplitude (completed by the low-energy constants $\bar{d}_j$). Only those parts of the πN-scattering amplitude, which are either independent of the pion CMS energy ω or depend on it linearly could be treated with the techniques available. The contributions are, in general, small. Below, we present only the larger portions within this class. The omitted pieces are about one order of magnitude smaller. To facilitate a better understanding, we have subdivided this class into subclasses labeled by roman numerals, following Refs. [7,15].

The auxiliary function

$$G(w) = \left[1 + 2g_A^2 - \frac{w^2}{4}\left(1 + 5g_A^2\right)\right]\frac{\sqrt{w^2-4}}{w}\ln\frac{w + \sqrt{w^2-4}}{2}$$
$$+ \frac{w^2}{24}\left(5 + 13g_A^2\right) - 1 - 2g_A^2 + 48\pi^2 f_\pi^2[(2-w^2)(\bar{d}_1 + \bar{d}_2) + 4\bar{d}_5] \tag{2.32}$$

arises from the part linear in ω of the isovector non-spin-flip πN amplitude $g^-(\omega,t)$ with $t = (wm_\pi)^2$ (see, e.g., Appendix B in Ref. [20]). The spectral functions derived from this selected set of 3π-exchange diagrams read as follows.

Class Xb:

$$\mathrm{Im}W_S = \frac{g_A^2 m_\pi^6}{(4f_\pi)^8\pi^5}\int_2^{u-1} dw\,\frac{4G(w)}{27w^2u^4}[(w^2-4)\lambda(w)]^{3/2}, \tag{2.33}$$

$$\mathrm{Im}(\mu^2 W_T - W_S) = \frac{g_A^2 m_\pi^6}{(4f_\pi)^8\pi^5}\int_2^{u-1} dw\,\frac{4G(w)}{9w^2u^4}(w^2-4)^{3/2}\sqrt{\lambda(w)}\,\frac{3u^2+1}{u^2-1}[u^4 - (w^2-1)^2]. \tag{2.34}$$

Class XIb:

$$\mathrm{Im}W_S = \frac{g_A^2 m_\pi^6}{(4f_\pi)^8\pi^5}\int_2^{u-1} dw\,\frac{8G(w)}{27w^2u^4}(w^2-4)^{3/2}\sqrt{\lambda(w)}\,[2u^2(1+7w^2)-u^4-(w^2-1)^2], \tag{2.35}$$

$$\mathrm{Im}(\mu^2 W_T - W_S) = \frac{g_A^2 m_\pi^6}{(4f_\pi)^8\pi^5}\int_2^{u-1} dw\,\frac{8G(w)}{9w^2u^4}\frac{(w^2-4)^{3/2}}{\sqrt{\lambda(w)}}\,(u^2+1-w^2)^2[2w^2(1+3u^2)-w^4-(u^2-1)^2]. \tag{2.36}$$

Class XIIb:

$$\mathrm{Im}W_S = \frac{g_A^2 m_\pi^6}{9f_\pi^8(4\pi)^5}\iint_{z^2<1} d\omega_1 d\omega_2\, G(w)\big[(\omega_1^2+\omega_2^2-2)(1-3z^2)-5k_1k_2z\big], \tag{2.37}$$

$$\mathrm{Im}(\mu^2 W_T - W_S) = -\frac{g_A^2 m_\pi^6}{3f_\pi^8(4\pi)^5}\iint_{z^2<1} d\omega_1 d\omega_2\, G(w)\omega_1\omega_2\left[5+2z\left(\frac{k_1}{k_2}+\frac{k_2}{k_1}\right)\right], \tag{2.38}$$

setting $w=\sqrt{1+u^2-2u\omega_1}$.

Class XIIIb:

$$\mathrm{Im}V_S = \frac{g_A^4 m_\pi^6}{(4f_\pi)^8\pi^3u^3}\int_2^{u-1} dw\,2G(w)\lambda(w)(2-w^2), \tag{2.39}$$

$$\mathrm{Im}(\mu^2 V_T - V_S) = \frac{g_A^4 m_\pi^6}{(4f_\pi)^8\pi^3u^3}\int_2^{u-1} dw\,4G(w)(2-w^2)(1+u^2-w^2)^2, \tag{2.40}$$

$$\begin{aligned}\mathrm{Im}W_S = \frac{g_A^4 m_\pi^6}{3f_\pi^8(4\pi)^5}\iint_{z^2<1} d\omega_1 d\omega_2\, G(w)\Big\{&u(\omega_1+4\omega_2)-2-\frac{\omega_1^2+8\omega_2^2}{3}+z^2\big(\omega_1^2+4\omega_2^2-5\big)\\&+\frac{zk_2}{k_1}\big(4u\omega_1+\omega_1^2-5\big)+\frac{zk_1}{k_2}\big(u\omega_2+\omega_2^2-2\big)+\frac{\arcsin(z)}{\sqrt{1-z^2}}\left[\frac{k_1}{k_2}(1-u\omega_2)+z(1-u\omega_1)\right]\Big\},\end{aligned} \tag{2.41}$$

$$\begin{aligned}\mathrm{Im}(\mu^2 W_T - W_S) = \frac{g_A^4 m_\pi^6}{f_\pi^8(4\pi)^5}\iint_{z^2<1} d\omega_1 d\omega_2\,\frac{2\omega_1}{3}G(w)\Big\{&\frac{2\omega_2}{k_1^2}[\omega_1(u-\omega_2)-1]+u+2\omega_2\\&+\frac{zk_1\omega_2}{k_2}+\frac{zk_2}{k_1}(4u+\omega_1)+\omega_1\left(\frac{2zk_2}{k_1}\right)^2+\frac{\arcsin(z)}{k_1k_2\sqrt{1-z^2}}\left[(1+u^2)\left(\omega_1+\omega_2-\frac{u}{2}\right)-2u\omega_1\omega_2\right]\Big\},\end{aligned} \tag{2.42}$$

setting again $w=\sqrt{1+u^2-2u\omega_1}$.

Class XIVb:

$$\mathrm{Im}V_S = \frac{g_A^4 m_\pi^6}{(4f_\pi)^8\pi^3u^3}\int_2^{u-1} dw\,\frac{G(w)}{2}\,\lambda(w)[u^2+w^2+4(u^2-1)w^{-2}-5], \tag{2.43}$$

$$\mathrm{Im}(\mu^2 V_T - V_S) = \frac{g_A^4 m_\pi^6}{(4f_\pi)^8\pi^3u^3}\int_2^{u-1} dw\,G(w)(w^2-1-u^2)[w^4-2w^2(3+u^2)+(u^2-1)^2(1+4w^{-2})]\,. \tag{2.44}$$

C. Four-pion exchange at N^{5}LO

The exchange of four pions between two nucleons occurs for the first time at N^{5}LO. The pertinent diagrams involve three loops and only leading order vertices, which explains the sixth power in small momenta. Three-pion exchange with just leading order vertices turned out to be negligibly small [5,6], and so we expect four-pion exchange with leading order vertices to be even smaller. Therefore, we can safely neglect this contribution.

III. PERTURBATIVE *NN* SCATTERING IN PERIPHERAL PARTIAL WAVES

To obtain an idea of the physical relevance and implications of the contributions evaluated in Sec. II, we will now calculate the impact of these on elastic *NN* scattering in peripheral partial waves. Specifically, we will consider partial waves with orbital angular momentum $L \geqslant 4$ (i.e., G waves and higher), because polynomial terms up to sixth power do not make any contributions to these angular momentum states. The $L \geqslant 4$ partial waves are sensitive only to the nonpolynomial pion-exchange expressions governed by chiral symmetry.

The smallness of the phase-shifts in peripheral partial waves suggests that the calculation can be done perturbatively. This avoids the complications and possible model dependences (e.g., cutoff dependence) that the nonperturbative treatment with the Lippmann-Schwinger equation, necessary for low partial waves, is beset with.

Previous systematic investigations of peripheral partial waves have been conducted at N^{2}LO in Refs. [3,4], at N^{3}LO in

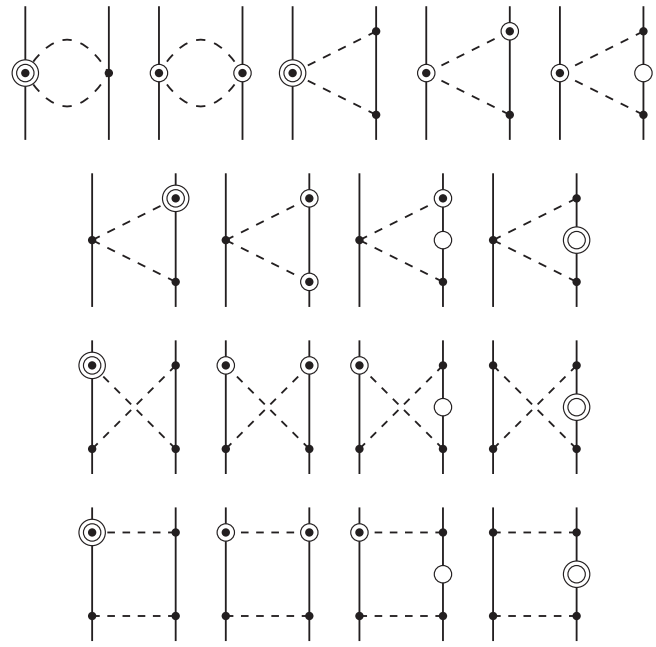

FIG. 2. Relativistic $1/M_N^2$ corrections to 2π-exchange diagrams that are counted as order 6. Notation as in Fig. 1. Open circles represent $1/M_N$ corrections.

Ref. [10], and at N^{4}LO in Ref. [15]. Here, we will now present the investigation at N^{5}LO.

The perturbative K matrix for neutron-proton (np) scattering is calculated as follows:

$$K(\vec{p}\,',\vec{p}) = V_{1\pi}^{(np)}(\vec{p}\,',\vec{p}) + V_{2\pi,\mathrm{it}}^{(np)}(\vec{p}\,',\vec{p}) + V_{3\pi,\mathrm{it}}^{(np)}(\vec{p}\,',\vec{p}) + V(\vec{p}\,',\vec{p}) \tag{3.1}$$

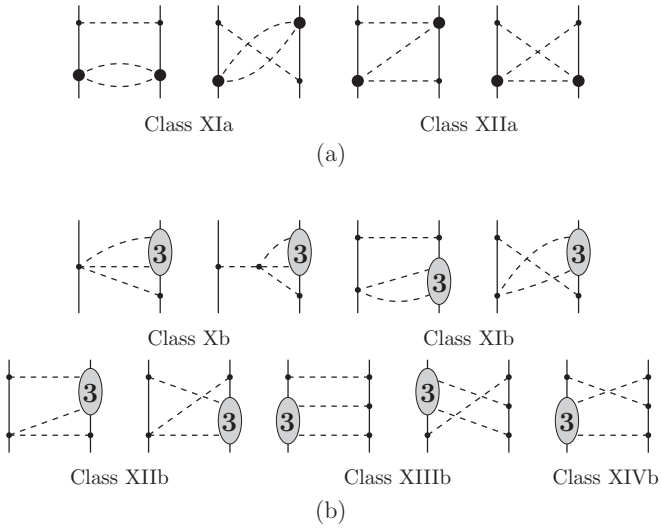

FIG. 3. Three-pion exchange contributions at N^{5}LO. (a) Diagrams proportional to c_i^2. (b) Diagrams involving the one-loop πN amplitude. Roman numerals refer to subclasses following the scheme introduced in Refs. [7,15]. Notation as in Fig. 1.

with $V_{1\pi}^{(np)}(\vec{p}\,',\vec{p}\,)$ the one-pion-exchange (1PE) potential that applies to np scattering taking charge-dependence into account. It is given by

$$V_{1\pi}^{(np)}(\vec{p}\,',\vec{p}\,) = -V_{1\pi}(m_{\pi^0}) + (-1)^{I+1}\,2\,V_{1\pi}(m_{\pi^\pm}), \tag{3.2}$$

where $I = 0,1$ denotes the total isospin of the pn system and

$$V_{1\pi}(m_\pi) = -\frac{g_A^2}{4f_\pi^2}\,\frac{\vec{\sigma}_1\cdot\vec{q}\;\vec{\sigma}_2\cdot\vec{q}}{q^2+m_\pi^2}\,. \tag{3.3}$$

We use the values $m_{\pi^0} = 134.9766$ MeV and $m_{\pi^\pm} = 139.5702$ MeV for the neutral and charged pion masses. $V_{2\pi,\mathrm{it}}^{(np)}(\vec{p}\,',\vec{p}\,)$ represents the once-iterated 1PE given by

$$V_{2\pi,\mathrm{it}}^{(np)}(\vec{p}\,',\vec{p}\,) = \mathcal{P}\int\frac{d^3p''}{(2\pi)^3}\,\frac{M_N^2}{E_{p''}}\,\frac{V_{1\pi}^{(np)}(\vec{p}\,',\vec{p}\,'')\,V_{1\pi}^{(np)}(\vec{p}\,'',\vec{p}\,)}{p^2-p''^2}, \tag{3.4}$$

where $\mathcal{P}$ denotes the principal value and $E_{p''} = \sqrt{M_N^2+p''^2}$. At sixth order, more iterations of 1π exchange should be included. However, we found that the difference between the once-iterated 1PE and the infinitely iterated 1PE is so small that it could not be identified on the scale of our phase shift figures. For that reason, we omit iterations of 1PE beyond what is contained in $V_{2\pi,\mathrm{it}}^{(np)}(\vec{p}\,',\vec{p}\,)$.

Furthermore, $V_{3\pi,\mathrm{it}}^{(np)}(\vec{p}\,',\vec{p}\,)$ stands for terms where irreducible 2PE is iterated with 1PE. At third order and higher, we include the iteration of the NLO 2PE with 1PE and, at fourth order and up, we include the iteration of the N^{2}LO 2PE with 1PE. We find irreducible 2PE of higher orders (N^{3}LO and N^{4}LO) iterated with 1PE to be negligible. The same applies to irreducible 3PE iterated with 1PE. Besides this, we have also iterated 2PE with 2PE; namely, NLO 2PE iterated with NLO 2PE, NLO 2PE iterated with N^{2}LO 2PE, NLO 2PE iterated with iterated 1PE, N^{2}LO 2PE iterated with iterated 1PE, and N3LO 2PE iterated with iterated 1PE. All iterations of 2PE with 2PE turn out to be negligible. In summary, the only non-negligible iterative contributions that involve more than two pions are the ones where an irreducible 2PE of order NLO or N^{2}LO is iterated with 1PE, which makes sense since contributions have to be of reasonably long range to contribute in a noticeable way in G and higher partial waves. Again, those latter ones we include and denote them symbolically by $V_{3\pi,\mathrm{it}}^{(np)}(\vec{p}\,',\vec{p}\,)$ in Eq. (3.1).

Finally, the third term on the right-hand side of Eq. (3.1), $V(\vec{p}\,',\vec{p}\,)$, stands for the sum of irreducible multipion exchange contributions that occur at the order up to which the calculation is conducted. In multipion exchanges, we use the average pion mass $m_\pi = 138.039$ MeV and, thus, neglect the charge dependence due to pion-mass splitting. For the average nucleon mass, we use twice the reduced mass of the pn system:

$$M_N = \frac{2M_pM_n}{M_p+M_n} = 938.9183\ \mathrm{MeV}. \tag{3.5}$$

Through relativistic kinematics, the CMS on-shell momentum p is related to the kinetic energy T_{lab} of the incident neutron

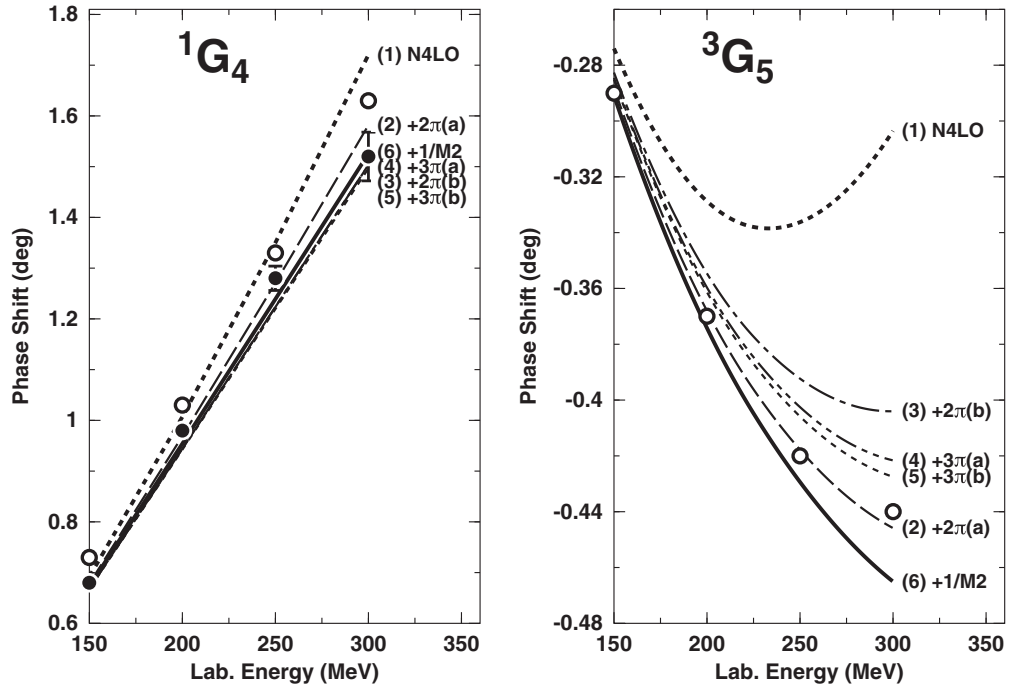

FIG. 4. Effect of individual sixth-order contributions on the neutron-proton phase shifts of two G waves. The individual contributions are added up successively in the order given in parentheses next to each curve. Curve (1) is N^{4}LO and curve (6) contains all N^{5}LO contributions calculated in this work. A SFR cutoff $\tilde{\Lambda} = 800$ MeV is applied. The filled and open circles represent the results from the Nijmegen multienergy np phase-shift analysis [28] and the GWU np analysis SP07 [29], respectively.

in the laboratory system, by

$$p^2 = \frac{M_p^2 T_{\rm lab}(T_{\rm lab} + 2M_n)}{(M_p + M_n)^2 + 2T_{\rm lab} M_p}, \tag{3.6}$$

with $M_p = 938.2720$ MeV and $M_n = 939.5654$ MeV the proton and neutron masses, respectively. The K matrix, Eq. (3.1), is decomposed into partial waves following Ref. [22] and phase shifts δ_L are then calculated via

$$\tan\delta_L(T_{\rm lab}) = -\frac{M_N^2 p}{16\pi^2 E_p}\, p\, K_L(p,p)\,. \tag{3.7}$$

For more details concerning the evaluation of phase shifts, including the case of coupled partial waves, see Ref. [23] or the Appendix of Ref. [24].

Chiral symmetry establishes a link between the dynamics in the πN system and the NN system (through common low-energy constants). In order to check the consistency, we use the LECs for subleading πN couplings as determined in analyses of low-energy elastic πN scattering. Appropriate analyses for our purposes are contained in Refs. [20,25], where πN scattering has been calculated at fourth order using the same power-counting of relativistic $1/M_N$ corrections as in the present work. The authors of Ref. [20] performed two fits: one to the GW [26] and one to the KH [27] partial wave analysis resulting in the two sets of LECs listed in Table I. In our present work, we apply the LECs based upon the GW analysis because it includes all πN data up to 2006, while the KH analysis may be perceived as outdated since it is from 1986. Moreover, we absorb the Goldberger-Treiman discrepancy into an effective value of the nucleon axial-vector coupling constant $g_A = g_{\pi NN} f_\pi / M_N = 1.29$.

As shown in Figs. 1 to 3 and derived in Sec. II, the sixth-order corrections consists of several contributions. We will now demonstrate how the individual sixth-order contributions impact NN phase shifts in peripheral waves. For this purpose, we display in Fig. 4 phase shifts for two peripheral partial waves, namely, $^1G_4$ and $^3G_5$. In each frame, the following curves are shown:

(1) N^{4}LO (as defined in Ref. [15]).
(2) The previous curve plus the N^{5}LO 2π-exchange contributions of class (a); Fig. 1(a) and Sec. II A 1.
(3) The previous curve plus the N^{5}LO 2π-exchange contributions of class (b); Fig. 1(b) and Sec. II A 2.
(4) The previous curve plus the N^{5}LO 3π-exchange contributions of class (a); Fig. 3(a) and Sec. II B 1.
(5) The previous curve plus the N^{5}LO 3π-exchange contributions of class (b); Fig. 3(b) and Sec. II B 2.
(6) The previous curve plus the $1/M_N^2$ corrections (denoted by "1/M2"); Fig. 2 and Sec. II A 4.

In summary, the various curves add up successively the individual N^{5}LO contributions in the order indicated by the curve labels. The last curve in this series, curve (6), includes all N^{5}LO contributions calculated in this paper. For all curves of this figure a SFR cutoff $\tilde{\Lambda} = 800$ MeV [cf. Eq. (2.2)] is employed.

From Fig. 4, we make the following observations. The two-loop 2π-exchange class (a), Fig. 1(a), generates a strong repulsive central force through the spectral function Eq. (2.3), while the spin-spin and tensor forces provided by this class, Eq. (2.4), are negligible. The fact that this class produces

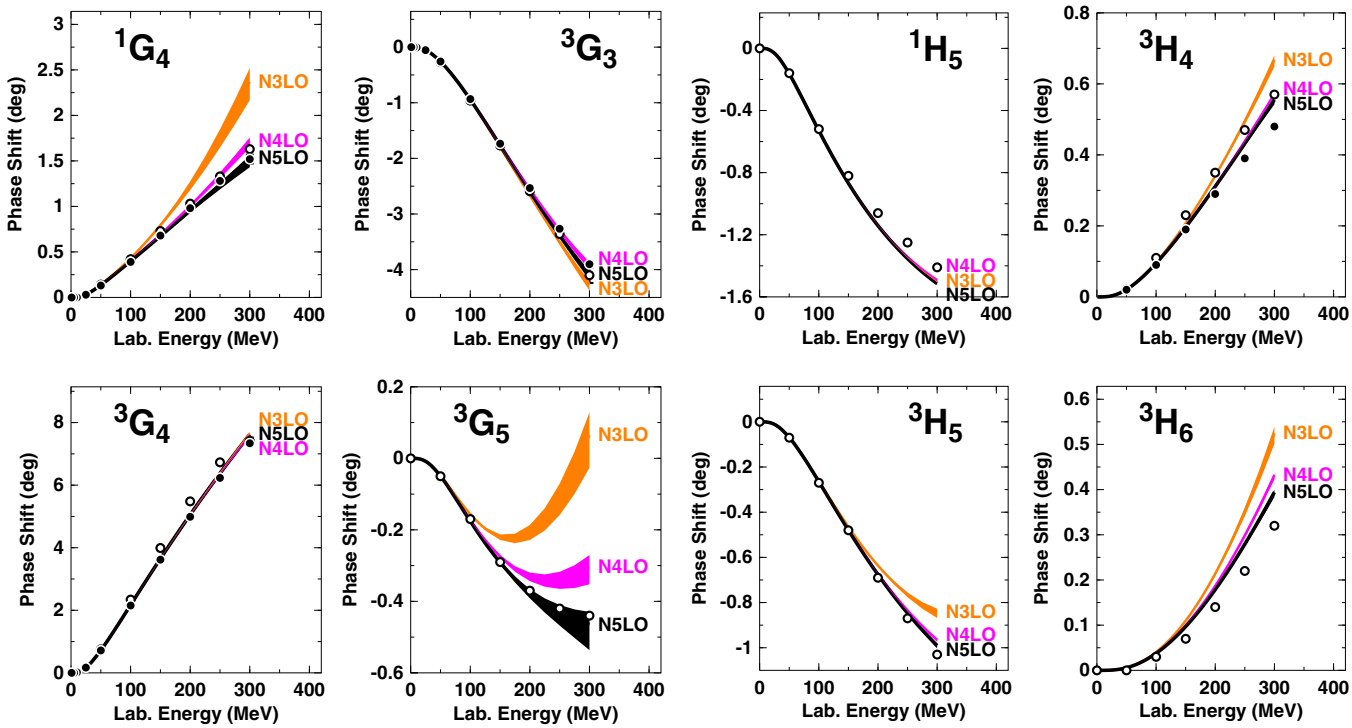

FIG. 5. (Color online) Phase-shifts of neutron-proton scattering in G and H waves at various orders as denoted. The shaded (colored) bands show the variations of the predictions when the SFR cutoff $\tilde{\Lambda}$ is changed over the range 700 to 900 MeV. Empirical phase shifts are as in Fig. 4.

a relatively large contribution is not unexpected, since it is proportional to c_i^2. The 2π-exchange contribution class (b), Fig. 1(b), creates a moderately repulsive central force as seen by its effect on $^1G_4$ and a noticeable tensor force, as the impact on $^3G_5$ demonstrates. The 3π-exchange class (a), Fig. 3(a), is negligible in $^1G_4$, but noticeable in $^3G_5$ and, therefore, it should not be neglected. This contribution is proportional to c_i^2, which suggests a non-negligible size but it is typically smaller than the corresponding 2π-exchange contribution class (a). The 3π-exchange class (b) contribution, Fig. 3(b), turns out to be negligible [see the difference between curve (4) and (5) in Fig. 4]. This may not be unexpected since it is a three-loop contribution with only leading-order vertices. Finally the relativistic $1/M_N^2$ corrections to the leading 2π exchange, Fig. 2, have a small but non-negligible impact, particularly in $^3G_5$.

The predictions for all G and H waves, are displayed in Fig. 5 in terms of shaded (colored) bands that are generated by varying the SFR cutoff $\tilde{\Lambda}$ [cf. Eq. (2.2)] between 700 and 900 MeV. The figure clearly reveals that, at N^{3}LO, the predictions are, in general, too attractive. As demonstrated in Ref. [15], the N^{4}LO contribution, essentially, compensates this attractive surplus. Now, let us turn to the new result at N^{5}LO: it shows a moderate repulsive contribution bringing the final prediction right onto the data (i.e., empirical phase-shifts). Moreover, the N^{5}LO contribution is, in general, substantially smaller than the one at N^{4}LO, thus, showing a signature of convergence of the chiral expansion.

Concerning the $^3G_5$ phase shifts, a comment is in place. From Fig. 5, it may appear that in this case the order-by-order convergence pattern is poor and the spread as a function of $\tilde{\Lambda}$ rather large and not shrinking with increasing order. Notice, however, that we are talking here about very small numbers: the whole phase shift scale of the $^3G_5$ frame is 0.8 deg and the spread as a function of $\tilde{\Lambda}$ is about 0.1 deg in each order. Moreover, the $^3G_5$ is known to be exceptionally sensitive to dynamics at medium-to-short range. This has been noticed and discussed before; see, e.g., Ref. [10].

Let us also comment on the spread as a function of the SFR cutoff $\tilde{\Lambda}$ of the other phase shifts shown in Fig. 5. While this spread goes down from N^{3}LO to N^{4}LO, it stays about the same when moving from N^{4}LO to N^{5}LO. Note, though, that the spread at N^{4}LO and N^{5}LO is relatively small as compared to the lower orders. Nevertheless, on general grounds, one might have expected a further reduction of this cutoff dependence at N^{5}LO, which is, however, not happening. At this stage of our investigation, the reason is not clear and we have to leave this issue to future considerations.

Finally, we also like to make a note on the empirical phase shifts with which we compare our predictions in Figs. 4 to 7. We use the 1993 Nijmegen analysis [28] (represented by filled circles in the figures) and the GWU analysis from summer 2007 [29] (open circles). We have also considered the recent Granada NN analysis [30]. However, it turned out that, in general, the Granada and Nijmegen analyses are so close to each other that it does not make sense to show them separately. Therefore, concerning an alternative analysis, we decided for GWU [29], for two reasons. The GWU analysis is truly alternative to Nijmegen (and Granada), because it is not performed with a cleaned-up database; it uses

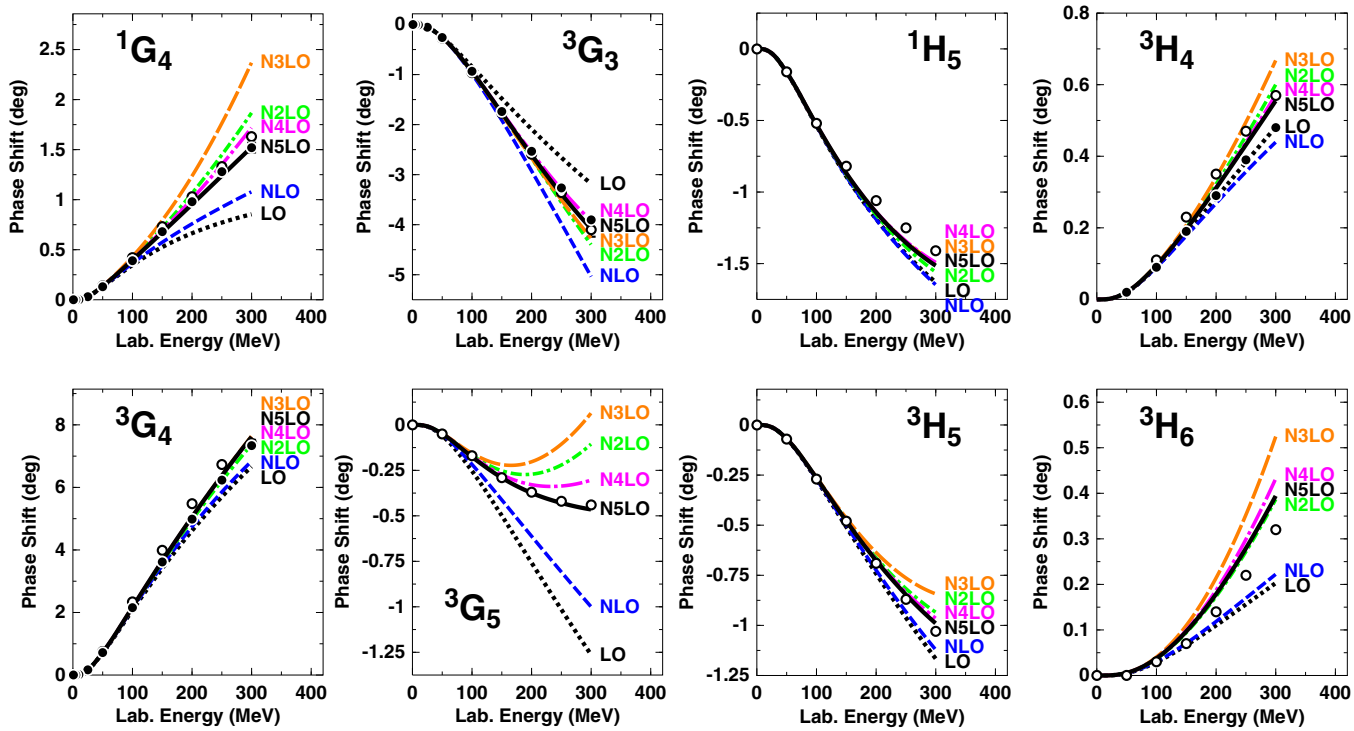

FIG. 6. (Color online) Phase-shifts of neutron-proton scattering in G and H waves at all orders from LO to N^{5}LO. A SFR cutoff $\tilde{\Lambda} = 800$ MeV is used. Empirical phase shifts are as in Fig. 4.

the full NN database. Moreover, the GWU analysis provides empirical phase shifts also for partial waves with $J = 5,6$, which we need. (The Nijmegen and Granada analyses stop at $J = 4$.)

Figure 5 includes only the three highest orders. However, a comparison between all orders is also of interest. Therefore, we show in Fig. 6 the contributions to phase shifts through all six chiral orders from LO to N^{5}LO (as defined in Ref. [15] and the present paper). Note that the difference between the LO prediction (one-pion-exchange, dotted line) and the data (filled and open circles) is to be provided by two- and three-pion exchanges, i.e., the intermediate-range part of the nuclear force. How well that is accomplished is a crucial test for any theory of nuclear forces. NLO produces only a small contribution, but N^{2}LO creates substantial intermediate-range attraction (most clearly seen in $^1G_4$, $^3G_5$, and $^3H_6$). In fact, N^{2}LO is the largest contribution among all orders. This is due to the one-loop 2π-exchange (2PE) triangle diagram which involves one $\pi\pi NN$-contact vertex proportional to c_i. This vertex represents correlated 2PE as well as intermediate $\Delta(1232)$-isobar excitation. It is well known from the traditional meson theory of nuclear forces [31–33] that these two features are crucial for a realistic and quantitative 2PE model. Consequently, the one-loop 2π exchange at N^{2}LO is attractive and assumes a realistic size, describing the intermediate-range attraction of the nuclear force about right. At N^{3}LO, more one-loop 2PE is added by the bubble diagram with two c_i vertices, a contribution that seemingly is overestimating the attraction. This attractive surplus is then compensated by the prevailingly repulsive two-loop 2π and 3π exchanges that occur at N^{4}LO and N^{5}LO.

In this context, it is worth noting that also in conventional meson theory [31] the one-loop models for the 2PE contribution always show some excess of attraction (cf. Figs. 7–9 of Ref. [10]). The same is true for the dispersion theoretic approach pursued by the Paris group [32,33]. In conventional meson theory, the surplus attraction is reduced by heavy-meson exchange (ρ and ω exchange) which, however, has no place in chiral effective field theory (as a finite-range contribution). Instead, in the latter approach, two-loop 2π and 3π exchanges provide the corrective action.

We now turn to Fig. 7, where we show how the six chiral orders impact the mixing angles with $J = 4,5$. Note that the mixing angles depend only on the tensor force [the quadratic spin-orbit term $V_{\sigma L}$ in Eq. (2.16) is very small]. It is clearly seen that the 1π exchange (LO) alone describes these mixing

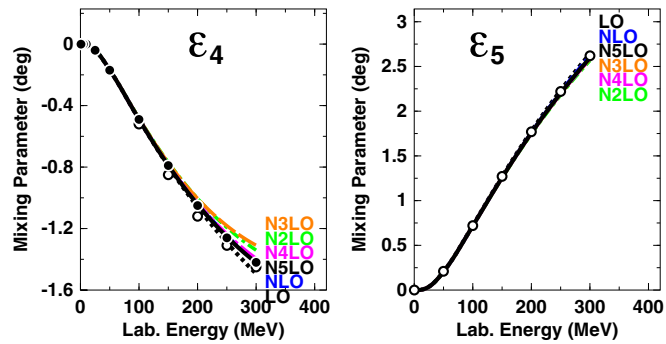

FIG. 7. (Color online) Mixing angles for neutron-proton scattering for $J = 4,5$ at all orders from LO to N^{5}LO. A SFR cutoff $\tilde{\Lambda} = 800$ MeV is used. Filled and open circles are as in Fig. 4.

angles correctly and that the various higher orders make only negligible contributions, particularly, for $J = 5$. At any order in the chiral expansion, tensor forces are created, but obviously the tensor force contributions beyond LO are of shorter range such that they do not matter in peripheral waves with $L \geqslant 4$.

IV. CONCLUSIONS

In this paper, we have calculated dominant 2π- and 3π-exchange contributions to the NN interaction which occur at N^5LO (sixth order) of the chiral low-momentum expansion. The calculations are done in heavy-baryon chiral perturbation theory using the most general fourth-order Lagrangian for pions and nucleons. We apply low-energy constants for subleading πN coupling, which were determined from an analysis of elastic πN scattering to fourth order using the same power counting scheme as in the present work. The spectral functions, which determine the NN amplitudes via subtracted dispersion integrals, are regularized by a cutoff $\tilde{\Lambda}$ in the range 0.7 to 0.9 GeV. Besides the cutoff $\tilde{\Lambda}$, our calculations do not involve any adjustable parameters.

Recent work on NN scattering in chiral perturbation theory [15] had revealed that the N^2LO, N^3LO, and N^4LO contributions are all about of the same size, thus raising some concern about the convergence of the chiral expansion for the NN potential. Our present calculations show that the contribution at N^5LO is substantially smaller than the one at N^4LO, thus, indicating a signature of convergence. The two-loop 2π-exchange contribution is the largest, while the corresponding three-loop contribution is small, but not negligible. Three-pion exchange is generally small at this order. The phase-shift predictions in G and H waves, where only the nonpolynomial terms governed by chiral symmetry contribute, are in excellent agreement with the data.

This investigation represents the most comprehensive (and successful) test of the implications of chiral symmetry for the NN system.

ACKNOWLEDGMENTS

This work was supported in part by the US Department of Energy under Grant No. DE-FG02-03ER41270 (R.M. and Y.N.), the Ministerio de Ciencia y Tecnología under Contract No. FPA2013-47443-C2-2-P and the European Community-Research Infrastructure Integrating Activity "Study of Strongly Interacting Matter" (HadronPhysics3 Grant No. 283286) (D.R.E.), and by DFG and NSFC (CRC110) (N.K.).

[1] S. Weinberg, Phys. Lett. B **251**, 288 (1990); Nucl. Phys. B **363**, 3 (1991).
[2] C. Ordóñez, L. Ray, and U. van Kolck, Phys. Rev. Lett. **72**, 1982 (1994); Phys. Rev. C **53**, 2086 (1996).
[3] N. Kaiser, R. Brockmann, and W. Weise, Nucl. Phys. A **625**, 758 (1997).
[4] N. Kaiser, S. Gerstendörfer, and W. Weise, Nucl. Phys. A **637**, 395 (1998).
[5] N. Kaiser, Phys. Rev. C **61**, 014003 (1999).
[6] N. Kaiser, Phys. Rev. C **62**, 024001 (2000).
[7] N. Kaiser, Phys. Rev. C **63**, 044010 (2001).
[8] N. Kaiser, Phys. Rev. C **64**, 057001 (2001).
[9] N. Kaiser, Phys. Rev. C **65**, 017001 (2001).
[10] D. R. Entem and R. Machleidt, Phys. Rev. C **66**, 014002 (2002).
[11] D. R. Entem and R. Machleidt, Phys. Rev. C **68**, 041001 (2003).
[12] E. Epelbaum, W. Glöckle, and U.-G. Meißner, Nucl. Phys. A **637**, 107 (1998); **671**, 295 (2000).
[13] E. Epelbaum, W. Glöckle, and U.-G. Meißner, Nucl. Phys. A **747**, 362 (2005).
[14] A. Ekström, G. Baardsen, C. Forssen, G. Hagen, M. Hjorth-Jensen, G. R. Jansen, R. Machleidt, W. Nazarewicz, T. Papenbrock, J. Sarich, and S. M. Wild, Phys. Rev. Lett. **110**, 192502 (2013).
[15] D. R. Entem, N. Kaiser, R. Machleidt, and Y. Nosyk, Phys. Rev. C **91**, 014002 (2015).
[16] M. Piarulli, L. Girlanda, R. Schiavilla, R. Navarro Pérez, J. E. Amaro, and E. Ruiz Arriola, Phys. Rev. C **91**, 024003 (2015).
[17] N. Kaiser, Phys. Rev. C **92**, 024002 (2015).
[18] R. Machleidt and D. R. Entem, Phys. Rep. **503**, 1 (2011).
[19] E. Epelbaum, H.-W. Hammer, and U.-G. Meißner, Rev. Mod. Phys. **81**, 1773 (2009).
[20] H. Krebs, A. Gasparyan, and E. Epelbaum, Phys. Rev. C **85**, 054006 (2012). We thank H. Krebs for pointing out and clarifying misprints in this paper.
[21] E. Epelbaum, W. Glöckle, and U.-G. Meißner, Eur. Phys. J. A **19**, 125 (2004).
[22] K. Erkelenz, R. Alzetta, and K. Holinde, Nucl. Phys. A **176**, 413 (1971).
[23] R. Machleidt, in *Computational Nuclear Physics 2 – Nuclear Reactions*, edited by K. Langanke, J. A. Maruhn, and S. E. Koonin (Springer, New York, 1993), p. 1.
[24] R. Machleidt, Phys. Rev. C **63**, 024001 (2001).
[25] K. A. Wendt, B. D. Carlsson, and A. Ekström, arXiv:1410.0646.
[26] R. A. Arndt, W. J. Briscoe, I. I. Strakovsky, and R. L. Workman, Phys. Rev. C **74**, 045205 (2006).
[27] R. Koch, Nucl. Phys. A **448**, 707 (1986).
[28] V. G. J. Stoks, R. A. M. Klomp, M. C. M. Rentmeester, and J. J. de Swart, Phys. Rev. C **48**, 792 (1993).
[29] W. J. Briscoe, I. I. Strakovsky, and R. L. Workman, SAID Partial-Wave Analysis Facility, Data Analysis Center, The George Washington University, solution SP07, Spring 2007 (unpublished).
[30] R. Navarro Pérez, J. E. Amaro, and E. Ruiz Arriola, Phys. Rev. C **88**, 064002 (2013).
[31] R. Machleidt, K. Holinde, and Ch. Elster, Phys. Rep. **149**, 1 (1987).
[32] R. Vinh Mau, in *Mesons in Nuclei*, Vol. I, edited by M. Rho and D. H. Wilkinson (North-Holland, Amsterdam, 1979), p. 151.
[33] M. Lacombe, B. Loiseau, J. M. Richard, R. Vinh Mau, J. Côté, P. Pirès, and R. de Tourreil, Phys. Rev. C **21**, 861 (1980).